Direct Correlation between Ultrafast Injection and Photoanode Performance in Quantum Dot Sensitized Solar Cells

ARTICLE *in* THE JOURNAL OF PHYSICAL CHEMISTRY C · DECEMBER 2010

Impact Factor: 4.77 · DOI: 10.1021/jp108499h

Direct Correlation between Ultrafast Injection and Photoanode Performance in Quantum Dot Sensitized Solar Cells

Néstor Guijarro,*,† Qing Shen,*,‡,§ Sixto Giménez,|| Iván Mora-Seró,|| Juan Bisquert,|| Teresa Lana-Villarreal,† Taro Toyoda,‡ and Roberto Gómez*,†

Institut Universitari d'Electroquímica i Departament de Química Física, Universitat d'Alacant, Apartat 99, E-03080 Alacant, Spain, Department of Engineering Science, Faculty of Informatics and Engineering, The University of Electro-Communications, 1-5-1 Chofugaoka, Chofu, Tokyo 182-8585, Japan, PRESTO, Japan Science and Technology Agency (JST), 4-1-8 Honcho Kawaguchi, Saitama 332-0012, Japan, and Grup de Dispositius Fotovoltaics i Optoelectrònics, Departament de Física, Universitat Jaume I, 12071 Castelló, Spain

Received: September 6, 2010; Revised Manuscript Received: November 1, 2010

The performance of quantum dot (QD) sensitized solar cells depends mainly on both electron injection from the QDs to the oxide matrix and recombination rates. Here we show a direct correlation between ultrafast carrier dynamics and photoanode (and complete solar cell) performance. TiO_2 nanoparticulate electrodes sensitized with colloidal CdSe QDs are prepared by either direct or linker-assisted adsorption (using cysteine, *p*-mercaptobenzoic acid, and mercaptopropionic acid). These electrodes are examined by ultrafast carrier dynamics, photopotential, and incident photon-to-current efficiency measurements to unravel factors controlling the efficiency in a closed solar cell. Subpicosecond time-resolved measurements are carried out by means of a lens-free heterodyne transient grating technique. In general, faster electron injection is observed for QDs directly adsorbed on TiO_2, which correlates with a better cell performance. Otherwise, increasingly faster electron injection is obtained as QD size decreases, regardless the mode of attachment. Photopotential measurements are performed in either sulfite or polysulfide solutions, in order to isolate different recombination pathways. The slowest recombination is reported for direct adsorption, whereas cysteine-mediated adsorption shows faster recombination. This study stresses the utility of ultrafast kinetic characterization in the development of efficient photoconverter devices.

Introduction

Over the last few decades, much effort has been focused on efficiently exploiting solar energy, in light of growing concern over global warming and strong dependence on fossil fuels. As a result, a new generation of solar cells based on low cost and engineering of nanomaterials has burst in the field of photovoltaics. One of the most promising concepts is the so-called quantum dot sensitized solar cell (QDSC). The sensitization of large band gap semiconductors (oxides) with lower band gap semiconductors dates back from the 1980s.[1,2] Systematic studies along these lines appeared in the 1990s together with the first QDSCs. Initially, chalcogenide QDs, directly grown into a TiO_2 nanoporous layer by either chemical or electrochemical methods, were used as sensitizers.[3−5] The first solar cell based on presynthesized QDs attached to the oxide via a linker (bifunctional molecule) was based on InP QDs attached to TiO_2 through thiolactic acid linkers.[6] QDSCs emerged as a modified version of the well-known DSCs, replacing dyes by semiconductor QDs,[7] in order to take advantage of their unique properties:[8,9] (1) tunable band gap, (2) extinction coefficients larger than those of dyes, and (3) the possibility of attaining quantum yields greater than unity by multiple exciton generation (MEG). Nevertheless, despite the potential of QDSCs, up to now, efficiencies (about 4%)[10−12] are significantly lower than those of dye sensitized solar cells (DSCs) (11.4%).[13] This fact requires a methodical investigation focused on the interfacial processes that occur under operating conditions as a starting point to enhance the performance of devices. In principle, QDSCs may benefit from intense efforts performed for the development of DSCs. However, specific analysis in QDSCs is required for further improvement, due to the different features of dyes and QDs. A wide variety of QDs has been tested in QDSCs (such as CdS,[14] CdSe,[15−18] PbS,[14] PbSe,[19] and InP[6,20]), but the large majority of reports involve CdSe QDs because of their easy preparation, stability, and promising results.[10,12]

Efficient sensitization requires a homogeneous high coverage of CdSe QDs at the nanoporous oxide surface (e.g., TiO_2, ZnO, ...), preventing both multilayer adsorption and the blockage of nanochannels. The modification of nanoporous TiO_2 has been carried out using mostly two strategies. On the one hand, previously synthesized QDs (by solvothermal or hot injection methods) can be adsorbed on the TiO_2 surface either directly[21,23] or using molecular wires (linkers).[21,24,25] In this case, QDs are protected by surfactant or linker molecules, minimizing the density of surface states that can play a key role in recombination pathways. On the other hand, direct growth of QDs has been achieved by either successive ionic layer adsorption-reaction (SILAR)[10,26−28] or chemical bath deposition (CBD).[29] Although these methods enable direct contact between electron donor (QD) and acceptor (TiO_2), favoring electron transfer, the lack of capping agents leads to a QD bare surface completely exposed to the electrolyte, thus providing a significant route of recombination. In addition, with these methods it is not possible to

* Corresponding authors: nestor.guijarro@ua.es (N.G.); shen@pc.uec.ac.jp (Q.S.); roberto.gomez@ua.es (R.G.).
† Universitat d'Alacant.
‡ The University of Electro-Communications.
§ PRESTO, Japan Science and Technology Agency.
|| Universitat Jaume I.

10.1021/jp108499h
Published on Web 12/02/2010

separately control QD size and coverage, giving rise to a broad distribution of QD sizes.

The performance of a QDSC dramatically depends on the relation among the rates of electron injection (from QDs to the oxide) and hole injection (into the electrolyte or hole transporting material (HTM)), and the different rates of recombination (QD internal recombination, recombination via TiO_2/QD, TiO_2/electrolyte or QD/electrolyte interfaces).[30] Time-resolved techniques have frequently been employed to monitor carrier dynamics inside CdSe QDs with the aim of clarifying the relative rates of the processes mentioned above. Measurements in colloidal CdSe QDs prove that, upon excitation, nonradiative relaxation of electron and holes to the conduction and valence band edges occurs in 200−400 fs and around 1.5 ps,[31] respectively. Radiative recombination from band edge states takes nanoseconds or longer.[32] Furthermore, electron trapping in surface states occurs in <100 ps, whereas hole trapping exhibits times ranging from 0.5 to 2 ps.[33] It should be noted that previous results indicate that the relaxation due to hole trapping is unaffected by surface modification, proving that NC intrinsic states are involved in this relaxation rather than surface states.[34] Ultrafast carrier dynamics has also been examined in CdSe−TiO_2 assemblies.[35] Generally, electron injection from QDs to TiO_2 occurs on a time scale of $10^{-7}-10^{-11}$ s.[16,36−38] Specifically, for CdSe QDs, linker-mediated adsorption using MPA yields size-dependent k_{et} (electron transfer rate constant) values of 10^7-10^{11} s^{-1} (QD size ranging from 2.4 to 7.5 nm).[17] Toyoda and co-workers have recently reported values about 5.4×10^9 s^{-1} for CdSe QDs (5.5 nm) grown on TiO_2 by CBD.[39] In addition, characteristic rate constants of $\sim 3 \times 10^9$ s^{-1} (2.4 nm) and $\sim 3 \times 10^8$ s^{-1} (4.2 nm) have been measured for the direct adsorption of colloidal core−shell CdSe-ZnS QDs.[40] In this context, the existence of reports dealing with the charge transfer mechanism in related systems can be mentioned.[41,42] Measurements of QD/MV^{2+} demonstrate remarkable ultrafast electron transfer times (~70 fs).[43] However, the number of publications dealing with hole injection to the electrolyte (or HTM) in the field of QDSCs is scarce. Recently, electron transfer rates of $\sim 8 \times 10^8$ s^{-1} in Na_2S[44] and $\sim 10^{11}$ s^{-1} in S_x^{2-} have been reported.[30] Despite this intensive work, we are not aware of a study establishing a direct correlation between ultrafast electron injection and the performance of the photoanode (or complete solar cell).

In this article, we focus on the relation between microscopic properties (ultrafast kinetics) and the ultimate macroscopic properties of a complete device (solar cell performance). We have employed colloidal QDs, which allow a higher control of nanocrystal size, studying the effect of both the mode of attachment and the size of CdSe QDs on charge separation in TiO_2 sensitized electrodes. The sensitization was performed either by direct or linker-assisted QD adsorption. We have applied a recently developed lens-free heterodyne detection transient grating (LF-HD-TG) technique to investigate the ultrafast carrier dynamics of photogenerated electrons and holes (on the picosecond time scale). Recombination of modified electrodes has been evaluated by photopotential measurements. Moreover, all these results have been correlated with power conversion efficiencies of complete devices.

Experimental Section

Synthesis of CdSe QDs. Colloidal dispersions of CdSe QDs capped with trioctylphosphine (TOP) were prepared by a solvothermal route which permits size control.[45] In this work, reaction time was fixed to 3, 5, and 15 h, in order to select different QD sizes.

Preparation of TiO_2 Electrodes. Nanoporous TiO_2 electrodes were prepared using either F-SnO_2 (FTO) coated glass or thermally treated Ti foil as substrates (Goodfellow, 99.6%; thickness = 0.1 mm). The latter was obtained as described previously.[28] TiO_2 films were prepared by spreading (doctor blading) 7 μL per cm^2 of an aqueous paste of Degussa P25 over either 1.4 cm^2 of FTO or 3.6 cm^2 of thermally treated Ti foil. This suspension was prepared by grinding a mixture of 1 g of TiO_2 powder, 2.0 mL of H_2O, 30 μL of acetylacetone (99+ %, Aldrich), and 20 μL of Triton X100 (Aldrich). The thickness of the film was measured to be ~5 μm by means of a profilometer (Dektak 3, Veeco).

Sensitization of TiO_2 Electrodes. Sensitized TiO_2 samples were prepared by two different methods. On the one hand, direct adsorption (DA) of CdSe QDs was achieved by immersion of TiO_2 electrodes in a CH_2Cl_2 (99.6%, Sigma Aldrich) CdSe QD dispersion, using soaking times ranging from 1 h to 1 week. On the other, linker-assisted adsorption (LA) was performed employing *p*-mercaptobenzoic acid (MBA, 90%, Aldrich), cysteine (97%, Aldrich), and mercaptopropionic acid (MPA, 99%, Aldrich) as molecular wires. First, the linker was anchored to the TiO_2 surface by immersion in saturated toluene solutions of cysteine (5 mM) or MBA (10 mM) for 24 h. Second, these electrodes were washed with pure toluene for $^1/_2$ h to remove the excess of the linker. Finally, the modified electrodes were transferred to a toluene CdSe QD dispersion for 3 days, to ensure QD saturation. The procedure for modification of TiO_2 with MPA has previously been reported by some of us.[21]

UV−vis Characterization. Absorption spectra were obtained with a Shimadzu UV-2401PC. In particular, diffuse reflectance spectra of sensitized TiO_2 electrodes were measured by means of an integrating sphere using $BaSO_4$ (Wako) as background. Kubelka−Munk transformation was undertaken to facilitate the analysis of the reflectance spectra.

Photoelectrochemical Measurements. Photoelectrochemical measurements were performed at room temperature in a three-electrode cell equipped with a fused silica window using a computer-controlled Autolab PGSTAT30 potentiostat. All potentials were measured against and are referred to a Ag/AgCl/KCl (sat.) reference electrode, whereas a Pt wire was used as counterelectrode. Two kinds of working electrolytes, either a 0.5 M Na_2SO_3 (98.0% min, Alfa Aesar) solution or a 1 M Na_2S (98%, Sigma Aldrich) + 0.1 M S (99.98%, Aldrich) + 1 M NaOH (99.0% min, Scharlau) solution (polysulfide), were used, both prepared in ultrapure water and N_2 purged before measurements. A 300 W Xe arc lamp (Osram) was used for electrode illumination from the substrate side (in the case of FTO glass). The light intensity was measured with an optical power meter (Oriel model 70310) equipped with a photodetector (thermo Oriel 71608). IPCE (incident-photon-to-current efficiency) measurements were performed placing a monochromator (Oriel model 74100) between the light source and the cell. The 300 W Xe arc lamp was equipped with a UV filter (cutoff $\lambda < 380$ nm), a water filter (to suppress IR radiation), and a neutral density filter (OD = 1) (irradiance: 50.4 $mW \cdot cm^{-2}$) for the photopotential experiments.

Configuration and Measurement of Solar Cells. Solar cells were prepared by assembling a sensitized TiO_2 electrode (photoanode) and a copper sulfide counterelectrode, using a silicone spacer (thickness ~50 μm) and a droplet (10 μL) of the polysulfide electrolyte. The active area of the cells was 0.24 cm^2. The photovoltaic characteristics of devices were measured

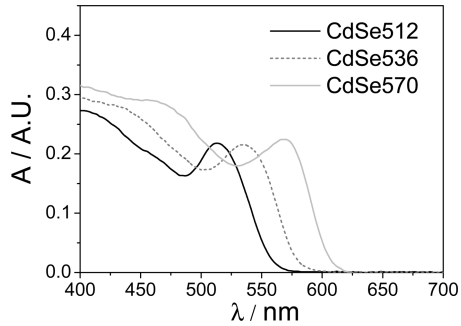

Figure 1. UV−vis absorption spectra of the CdSe colloidal dispersions used in this study.

by using a solar simulator (Peccell Technologies, Inc.) at 1 sun (AM 1.5G, 100 mW cm^{-2}).

TG Technique. The principle and setup of the lens-free heterodyne detection transient grating (LF-HD-TG) technique have been described in previous papers.[18,46−49] In this experiment, the laser source was a titanium/sapphire laser (CPA-2010, Clark-MXR Inc.) with a wavelength of 775 nm, a repetition rate of 1 kHz, and a pulse width of 150 fs. The typical laser pulse intensity used in the TG experiments was as low as 2 mW (2 μJ/pulse and the repetition frequency of the laser pulse is 1 kHz) although in some experiments it was increased up to 16 mW. The area of the laser beam on the sample was about 0.2 cm^2. Therefore, the typical pump light intensity was as low as 10 mW·cm^{-2}. The samples showed no apparent photodamage during the TG measurements. The light was separated into two parts. One of them was used as a probe pulse. The other was used to pump an optical parametric amplifier (OPA) (a TOAPS from Quantronix) to generate light pulses with a wavelength tunable from 290 nm to 3 μm used as pump light in the TG measurement. In this study, the pump pulse wavelength was 470 nm and the probe pulse wavelength was 775 nm.

Results and Discussion

Optical Properties of Colloidal QDs. Absorption spectra of the CdSe colloidal dispersions employed in this study are shown in Figure 1. Well-defined peaks at 570, 536, and 512 nm reveal a narrow size distribution centered at around 3.5, 2.8, and 2.5 nm, respectively.[50] In the following, colloidal dispersions are referred to as CdSe570, CdSe536, and CdSe512.

Ultrafast Carrier Dynamics Study. Time-resolved measurements have been carried out by means of LF-HD-TG technique. As described in depth elsewhere,[49] TG response monitors the change in the refractive index of the sample ($\Delta n(t)$) upon photoexcitation. Assuming Drude's model, the change in the refractive index as a function of time can be expressed as a linear function of the concentration of free photogenerated carriers (i.e., electrons and holes in the CdSe QDs $-N_{e,CdSe}$ or $N_{h,CdSe^-}$ and injected electrons in TiO_2-N_{e,TiO_2^-})

$$\Delta n(t) = \frac{1}{2n_{0,CdSe}}\left(\frac{-N_{e,CdSe}(t)e^2}{m_{e,CdSe}\omega_p{}^2\varepsilon_0}\right) + \frac{1}{2n_{0,CdSe}} \times \left(\frac{-N_{h,CdSe}(t)e^2}{m_{h,CdSe}\omega_p{}^2\varepsilon_0}\right) + \frac{1}{2n_{0,TiO_2}}\left(\frac{-N_{e,TiO_2}(t)e^2}{m_{e,TiO_2}\omega_p{}^2\varepsilon_0}\right) \quad (1)$$

where ω_p is the radial probe frequency, e is the elementary charge, ε_0 is free-space permittivity, and $n_{0,CdSe}$ (2.7)[51] and n_{0,TiO_2} (2.5) are the refractive indices of CdSe and TiO_2, respectively.

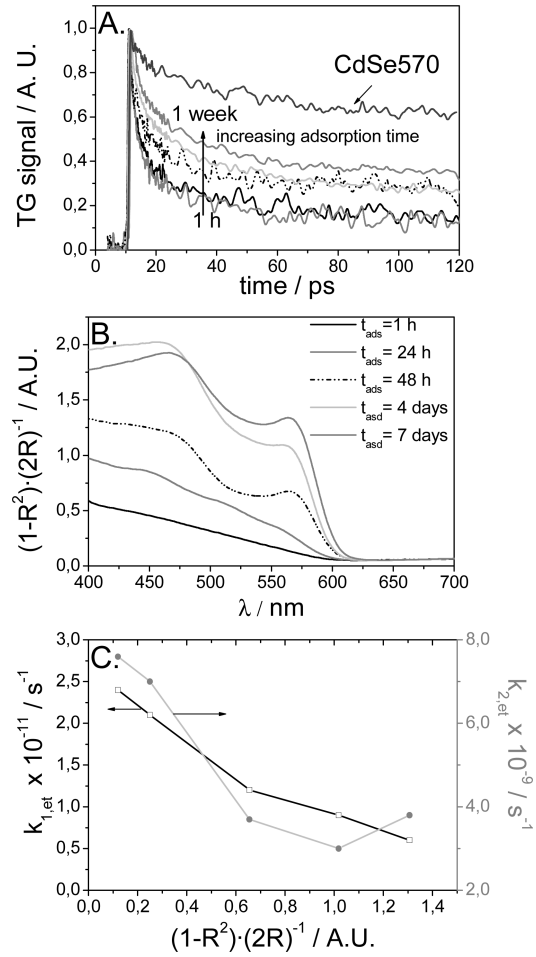

Figure 2. TG responses of a CdSe570 colloidal dispersion, and TiO_2 thin films modified by direct adsorption of CdSe570 for different adsorption times, all normalized to the maximum value (A). Kubelka−Munk transformation corresponding to the diffuse reflectance spectra (R) obtained for these samples (B). Electron transfer rate constants as a function of the Kubelka−Munk value measured at 570 nm (C).

It should be noted that the relative contribution of each carrier to the TG signal is inversely proportional to its corresponding effective mass (m_e, m_h). Taking into account the effective masses of electrons and holes in CdSe (0.13 m_0 and 0.44 m_0, respectively) and the effective mass of electrons in TiO_2 (30 m_0), the contribution of TiO_2 electrons to the TG signal can be neglected. As the effective mass of CdSe holes is more than 3 times that of CdSe electrons, the TG signal is dominated by the response of free electrons in CdSe, although the contribution from holes is not negligible (CdSe hole contribution accounts for one-fourth of the overall TG signal). It has been previously shown that the carrier depopulation mechanism, monitored by the TG technique, should be ascribed to one body processes (hole trapping and electron injection or trapping) under our experimental condition of very low pump intensity (2 mW).[39,46] In fact, the laser pulse intensity was changed from 2 to 16 mW to check the pump intensity dependence of the TG response. It was found that the dependence of the maximum signal intensity on the pump intensity was linear and that the waveforms of the responses overlapped with each other very well when they were normalized to the TG signal peak intensity.

The TG responses of both a colloidal dispersion CdSe570 and a film sensitized by direct adsorption (DA) using the same dispersion are shown in Figure 2A. In Figure 2B the Kubelka−Munk transformations of the reflectance spectra for

TABLE 1: Fitting Parameters of TG Response Curves (eq 2) and Calculated Electron Transfer Rate Constants (eq 3)

sample	A_1	τ_1 (ps)	A_2	τ_2 (ps)	$k_{1,et} \times 10^{-11}$ (s^{-1})	$k_{2,et} \times 10^{-9}$ (s^{-1})
CdSe570	0.18 ± 0.01	8.8 ± 0.8	0.77 ± 0.01	506 ± 45		
DA	0.66 ± 0.02	2.8 ± 0.2	0.30 ± 0.01	104 ± 8	2.4 ± 0.4	7.6 ± 0.9
			$t_{ads} = 1$ h			
DA	0.60 ± 0.02	3.1 ± 0.2	0.33 ± 0.01	111 ± 7	2.1 ± 0.3	7.0 ± 0.7
			$t_{ads} = 24$ h			
DA	0.52 ± 0.02	4.3 ± 0.4	0.42 ± 0.02	177 ± 26	1.2 ± 0.3	3.7 ± 1.0
			$t_{ads} = 48$ h			
DA	0.42 ± 0.02	4.8 ± 0.4	0.48 ± 0.01	202 ± 17	0.9 ± 0.3	3.0 ± 0.6
			$t_{ads} = 4$ days			
DA	0.48 ± 0.01	5.9 ± 0.3	0.46 ± 0.01	172 ± 8	$0.6 \pm 0,2$	3.8 ± 0.4
			$t_{ads} = 1$ week			
LA (cysteine)	0.46 ± 0.01	3.9 ± 0.3	0.41 ± 0.01	127 ± 7	1.4 ± 0.3	5.9 ± 0.6
LA (MPA)	0.50 ± 0.01	4.2 ± 0.2	0.46 ± 0.01	204 ± 13	1.2 ± 0.2	2.9 ± 0.5
LA (MBA)	0.38 ± 0.02	7.7 ± 0.3	0.77 ± 0.01	245 ± 24	0.2 ± 0.1	2.1 ± 0.6

the sensitized films are given. Spectra match quite well that of the colloidal dispersion CdSe570. The longer the adsorption time, the higher the quantum dot loading, leading to increasingly reddish electrodes. According to previous studies,[37−39] it seems appropriate to fit the relaxation of the TG signal to a double exponential decay

$$y = A_1 e^{-t/\tau_1} + A_2 e^{-t/\tau_2} \quad (2)$$

In fact, in all cases, the double exponential function fits quite well the transient experiment. The results of the fittings are shown in Table 1.

As mentioned above, in this scenario, and according to the values of the effective masses, contribution to TG signal from holes is about 30% of that from electrons in CdSe. Paying attention to the amplitude coefficients for the CdSe570 colloidal dispersion (A_1 and A_2) in Table 1, we observe that the A_1/A_2 value is about one-fourth. This suggests that depopulation processes involving photogenerated carriers in CdSe can be resolved in the time scale of the experiment, i.e., the fast decay contribution (A_1) can be solely associated to hole trapping, whereas the slow decay (A_2) should be ascribed to electron trapping, because no electron injection can occur in the colloidal dispersion. A similar interpretation was given by Shen and co-workers for CdSe QDs grown by CBD on glass.[39] Time constants obtained for hole trapping (~8 ps) and electron trapping (~500 ps) are slightly larger than those reported by Klimov, probably due to the different nature of the corresponding samples.[34]

Figure 2A shows that the adsorption of CdSe QDs on TiO_2 induces a decay of carrier concentration significantly faster than in colloidal medium, because electron transfer from QDs to TiO_2 arises as an additional depopulation pathway. For sensitized films, A_1/A_2 is larger than the expected value of 0.3. In addition, the characteristic times of the TG decay fitted with eq 2, τ_1 and τ_2, present lower values than those obtained for the colloidal dispersion; see Table 1. These results indicate that for sensitized films both components of the decay include electron transfer to TiO_2; i.e., fast and slow injections are resolved. This interpretation is supported by the fact that Blackburn and co-workers obtained similar decay profiles using transient absorption spectroscopy when monitoring the evolution of photogenerated electrons in CdS QDs grown by CBD on TiO_2.[37] In addition, we assume that the contribution from hole and electron trapping keep on being mainly associated to the fast decay and the slow decay, respectively. Figure 2A portrays a marked effect of the adsorption time on the decay curves. Qualitatively, shorter adsorption times yield faster depopulation of free carriers, i.e., faster electron injection. It should be noted that electron injection from CdSe QDs into TiO_2 presents a broad time distribution. Assuming that such an electron transfer process takes place by tunneling from the excited QD to TiO_2 (as it is widely accepted for these samples),[22] the distance between electron donor and acceptor should be a key parameter controlling the rate of injection. Herein, the fact that two contributions to the electron injection are distinguished likely reflects that there exists a distribution of distances QD−TiO_2 in the DA-modified samples. This is in agreement with a recent work,[21] in which the characterization of CdSe sensitized rutile single crystals by means of atomic force microscopy (AFM), revealed that the experimental conditions employed for DA sensitization favor a random mechanism of adsorption, leading to aggregation rather than to homogeneous monolayer adsorption. Therefore, a plausible interpretation for the TG signal for DA-sensitized samples implies that the fast component of the electron transfer could be ascribed to electron injection from QDs directly adsorbed on TiO_2 (first monolayer), whereas the slow component would be due to the injection from QDs that are not directly adsorbed on TiO_2.

In order to obtain the electron injection rate, one option consists in expressing each decay rate constant k_i ($k_i = 1/\tau_1$) as $k_i = k_{i,r} + k_{i,et}$, where $k_{i,r}$ is the intrinsic CdSe decay rate (mostly trapping) and $k_{i,et}$ is the electron transfer rate.[39] By assuming that the intrinsic decay rate constant in sensitized electrodes is the same as that in the CdSe colloidal dispersion, we can estimate the electron transfer rate constant from CdSe to TiO_2 as

$$k_{i,et} = \frac{1}{\tau_{i,adsorbed}} - \frac{1}{\tau_{i,dispersion}} \quad (3)$$

As illustrated in Figure 2C, both $k_{1,et}$ and $k_{2,et}$ transfer rate constants decrease steadily as the amount of adsorbed CdSe QDs increases. Otherwise, Table 1 shows that the amplitude A_2 increases as the adsorption progresses, in contrast with the behavior of A_1.

Concerning the amplitudes, the previously mentioned tendency to aggregation explains the increasingly lower values of the ratio A_1/A_2. In other words, as the adsorption progresses, the QD loading increases mainly in outer layers, rather than in

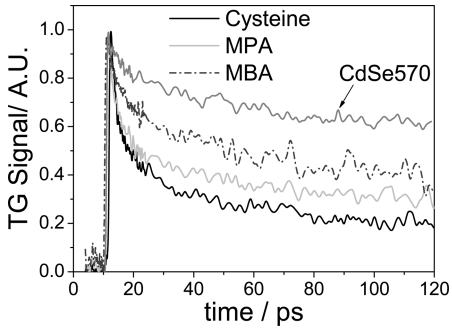

Figure 3. TG responses for CdSe-sensitized TiO_2 electrodes using cysteine, MPA, and MBA as linkers. All the curves are normalized to the maximum value. The TG response corresponding to the CdSe570 colloidal dispersion is also given for the sake of comparison.

the first monolayer, leading to a higher weight of the slow component. On the other hand, the progressive slowdown of the electron transfer rate constants would be ascribed again to the aggregation that accompanies the adsorption process. Specifically, the contact between QDs would induce the generation of electron traps that could delay electron injection. Electronic delocalization throughout aggregates could also hamper vectorial injection. Moreover, the increase in the mean distance QD-TiO_2, as the multilayer adsorption progresses, would also explain the observed decrease in the rate constant $k_{2,et}$. It should also be mentioned that, as discussed in depth by Hodes,[30] in the case of QD multilayers, the probability of injection from the QDs is expected to decrease as photogenerated electrons have to cross more QD−QD grain boundaries before reaching the TiO_2. Constant rates obtained are higher than those previously reported by Makhal and co-workers[40] for direct adsorption of CdSe−ZnS (3.8×10^8 s^{-1}, QD size 4.2 nm). In such a case, samples were prepared by stirring a mixture of QDs and TiO_2 nanoparticles and depositing a thin film. Hence, we consider that either this nonequilibrium adsorption of QDs favors aggregation or the ZnS capping shell hinders electron injection. As shown by Shen and co-workers,[39] directly grown CdSe QDs by CBD gives slower injection rates (5.4×10^9 s^{-1}, average QD size 5.5 nm), because of both the numerous QD/QD interfaces and the larger QD size (see below). Otherwise, we have recently reported in situ grown CdSe QDs by the SILAR method.[28] Results show slightly shorter characteristic times, indicating that close and intimate contact QD/oxide enhances electron transfer.

Figure 3 displays the TG responses for TiO_2 thin films modified by linker-adsorbed (LA) CdSe570 QDs. Figure S1 in the Supporting Information shows their corresponding UV−vis spectra after the Kubelka−Munk transformation. In stark contrast with the DA case, TG signals are not sensitive to adsorption time (results not shown). We conclude that the specific interaction between the thiol group (−SH) of the linker and the QD leads to homogeneous adsorption, in which all the QDs are adsorbed directly on the oxide surface with no aggregation as in the DA case, as proved by AFM images.[21] Interestingly, strong dependence of the decay on the linker nature is observed in Figure 3, which suggests that, not only the length but also other factors such as the dipole moment, the redox properties, or the electronic structure of the linker may play a role in the carrier dynamics. The values obtained for the parameters of a biexponential fitting (eq 2) are given in Table 1, together with the electron transfer rate constants calculated according to eq 3. Kamat's group has extensively discussed electron transfer from CdSe to TiO_2 via MPA,[16,17,24] with values ranging from 1.0×10^9 to 2×10^{11} s^{-1}, in agreement with our results.

In the case of LA adsorption, in contrast with the DA method, aggregation can be neglected for the adsorption times employed in this study, and other factors should be invoked to explain the broad distribution of injection times. To date, the anchorage of the QDs to the oxide surface has not been characterized in detail, leaving the adsorption mechanism poorly understood. Therefore, a distribution of QD−TiO_2 distances could be expected because of the different number of molecular wires tethering the QD to the TiO_2 surface and the very heterogeneous nature of the nanoparticulate TiO_2 matrix. Taking into account that injection by tunneling is more effective as the distance QD−TiO_2 decreases, the observed fast and slow injection rates could again be ascribed to electron transfer from QDs located on average near or far from the oxide surface. Of course, we expect a distribution of distances, but the fact of mentioning two average distances is a consequence of the choice of a biexponential function for fitting the TG decay. Another interpretation, recently given by Dibbell et al., relies on considering a fast injection from the QD excited state and a slow one from trap states.[52] They reported that electron injection in CdS-sensitized TiO_2 using MBA as a linker occurs on a multiple time scale, i.e., a fast injection $<10^{-8}$ s and a slow injection $10^{-7}-10^{-6}$ s. Nonetheless, the corresponding injection rates are lower than commonly accepted values (including ours) for these systems. Lower time resolution of their technique (nanosecond) allows one to study processes different from those reported in this study. Nevertheless, our results could also be easily explained by considering that slow injection would involve a contribution from QD surface states or QD/linker interfacial states, discarding QD/QD interfacial states because the decay profiles are not sensitive to the adsorption time.

It is noteworthy that, in general, short-time direct adsorption yields faster electron injection than linker-mediated adsorption; see Table 1. Probably, as suggested previously,[21,53] when QDs are directly adsorbed, the capping agent (TOP) is partially removed, which enables quasi-direct contact with the TiO_2 surface. In any case, cysteine also shows a high transfer rate. This suggests that, apart from its dipolar moment that can drive electron injection, cysteine (smaller than TOP) could effectively displace TOP molecules further approaching electron donor and acceptor, and improving tunneling injection. It is also worth noting that in the case of cysteine, the attachment to the oxide is probably made via two different functional groups: the carboxylate and the amino groups, which also could favor a lower TiO_2−CdSe distance, together with a more intimate electronic contact between electron donor and acceptor. MPA presents an electron injection slower than that for cysteine, although relatively close if experimental errors are taken into account, while MBA presents the slowest injection rate of the studied systems.

Finally, the QD size effect on the TG response has also been evaluated (Figure 4). For this purpose, TiO_2 electrodes have been sensitized by direct and linker-assisted adsorption (MPA, MBA) using CdSe536 and CdSe512. In all cases, the smaller the QD, the faster the electron transfer. Robel et al.[17] reported similar results attaching QDs via MPA to TiO_2. They have stated that increasingly fast electron injection is in agreement with the conduction band shift occurring as the QD size decreases, which improves the driving force for electron transfer. This idea is strongly supported by our results, which show the same tendency regardless the type

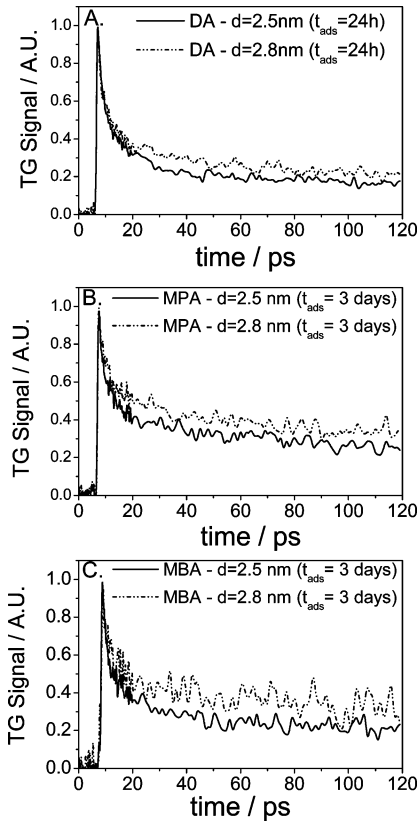

Figure 4. Effect of the QD size on the TG response for different attachment modes. Direct adsorption (A), as well as MPA- (B) and MBA-mediated (C) adsorption, of CdSe512 and CdSe536 are examined. All decays have been normalized to the maximum value.

of adsorption. As shown in Table S1 in the Supporting Information, in any case τ_1 and τ_2 become smaller as the QD size decreases (i.e., electron transfer is favored).

Photoelectrochemical Measurements and IPCE. Open circuit potential vs time curves are depicted in Figures 5A and 6. Open circuit potential values under illumination give a direct measurement of the steady-state concentration of electrons accumulated in the TiO_2 film by injection from photoexcited QDs. Potential relaxation upon illumination informs about electron recombination kinetics (electron lifetime).[54,55] Photopotential measurements of sensitized electrodes were obtained under different conditions to evaluate separately different recombination pathways.

Figure 5A shows experiments done in the absence of electron acceptors in solution. As shown, the stationary open circuit potential under illumination achieves increasingly negative values as follows:

$$\text{DA} > \text{MPA} > \text{MBA} > \text{cysteine}$$

On the other hand, potential relaxation kinetics after illumination is increasingly fast according to the tendency

$$\text{cysteine} > \text{MBA} > \text{MPA} > \text{DA}$$

In this experiment, potential decay (after illumination) is due to recombination between electrons (previously injected in TiO_2 from the QDs) and photogenerated holes trapped in

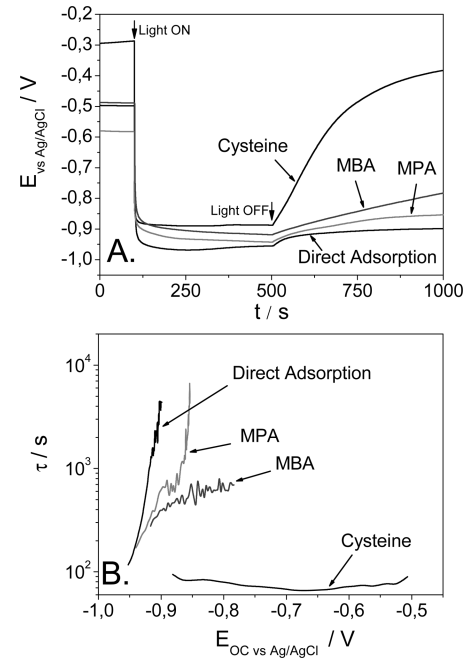

Figure 5. Photopotential measurements obtained for transient illumination of electrodes sensitized with CdSe570, using N_2-purged aqueous 0.5 M Na_2SO_3 as electrolyte (A). Electron lifetimes obtained from the open circuit potential decays after illumination for the different modes of attachment (B). All electrodes were prepared using thermally treated titanium foil as substrate.

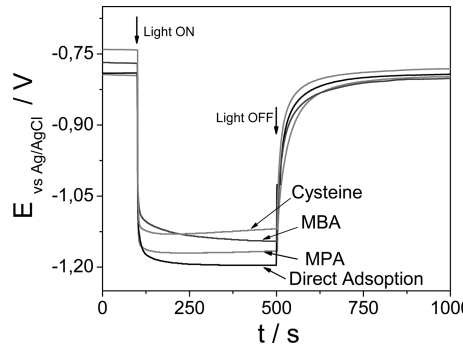

Figure 6. Photopotential measurements obtained for transient illumination of CdSe570 sensitized electrodes in aqueous 0.1 M S + 1 M Na_2S + 1 M NaOH. Electrodes were prepared using thermally treated titanium foil as substrate.

interfacial states (Scheme 1A). Electron lifetimes calculated according to

$$\tau = -n\left(\frac{\mathrm{d}n}{\mathrm{d}t}\right)^{-1} \tag{4}$$

where n is the electron density in the semiconductor nanostructure, have been plotted versus the open circuit potential[55] (see Figure 5B). As shown, the presence of linker molecules tethering the QD induces the generation of recombination centers, leading to electron lifetimes shorter than those obtained with DA. This is not unexpected as these linkers can efficiently trap photogenerated holes through generation of thyil radicals that could eventually recombine with electrons injected in TiO_2. At this point, it must be mentioned that τ values using an electrolyte containing sulfite are longer than those reported when using polysulfide.[23] This is also not unexpected, because the fast recombination

SCHEME 1: The Decay of Photopotential[a]

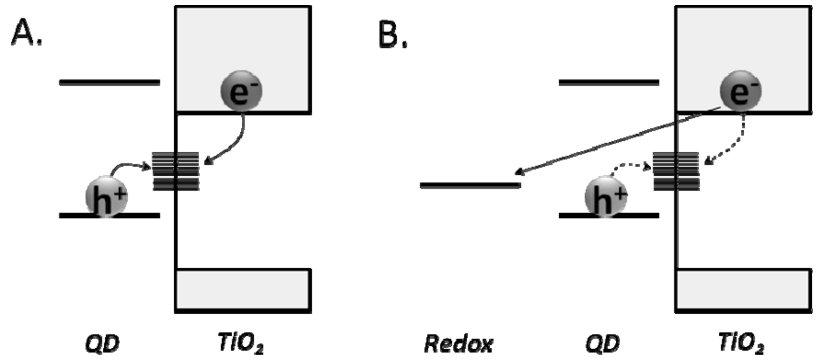

[a] The decay of photopotential when illumination is interrupted in sulfite solution relies on recombination between electrons accumulated in the TiO_2 and trapped holes at QD/TiO_2 interfaces (A). When polysulfide is employed as electrolyte, the decay of photopotential is mainly due to reaction with electrolyte species; in this case recombination with trapped holes is less probable (dashed line) (B).

pathway has been eliminated by the lack of a solution electron acceptor. Only slow recombination between electrons and trapped holes remains. When cysteine is used as a linker, an initial linear potential decay is obtained, giving rise to a constant and very low τ value. This fact suggests that this linker can induce a high density of hole trapping centers in the QD surface. This idea is supported by results obtained by Rajh and co-workers,[56] showing that photogenerated holes in TiO_2 nanoparticles were effectively scavenged by cysteine molecules adsorbed on their surface. We have recently reported similar open circuit potential decays for SILAR-sensitized samples, indicating a high density of interfacial states, which act as hole trapping and recombination centers.[28] Regarding MBA and MPA, the factors determining recombination kinetics are not clear. Maybe, the high electronic density of MBA together with its more negative redox potential could promote hole trapping in comparison to the case of MPA.

Experiments in the presence of a redox couple in solution (polysufide) have also been done; see Figure 6. In this case, the open circuit potential under illumination is increasingly negative according to

$$\text{DA} > \text{MPA} > \text{MBA} > \text{cysteine}$$

As expected photopotential decay when light is interrupted is much faster than without an electron scavenger, because recombination with the electrolyte dominates the signal relaxation (Scheme 1B). Electron lifetime has been plotted against E_{OC}, according to the procedure given by Zaban et al.[54] (see Figure S2 in the Supporting Information). Electron lifetime becomes larger as the potential increases and attains values within the usual range (1−100 s), as presented elsewhere.[23] However, no significant differences can be observed among sensitized samples on the time scale of our measurements. It must be stressed that relative values of steady-state open circuit potentials under illumination for different samples give information about recombination (mainly with the oxidized species of the redox couple). In other words, less negative open circuit potentials are expected as the leakage of electrons to the electrolyte (recombination) increases. Thereby, attaching QD directly to the TiO_2 surface diminishes recombination (as observed in experiments carried out in sulfite electrolyte). This result supports the notion that TOP molecules removed from the QD surface during direct adsorption could passivate the TiO_2 surface.

Experiments undertaken with bare TiO_2 electrodes with and without UV illumination were done to confirm that the decay observed when interrupting the light is mainly due to the introduction of quantum dots,[28] excluding a significant role of oxygen traces in the case of the sulfite solution.

The performance of a photoanode (or solar cell) can be characterized by the incident photon-to-current conversion efficiency (IPCE), corresponding to the number of electrons measured as photocurrent in the external circuit divided by the monochromatic photon flux that strikes the photoanode. This key parameter, depending on the illumination wavelength λ, can be expressed as the product[57]

$$\text{IPCE}(\lambda) = \text{LHE}(\lambda)\phi_{\text{inj}}\eta_{\text{coll}} \quad (5)$$

where LHE(λ) is the light-harvesting efficiency, ϕ_{inj} is the quantum yield for electron injection from the excited sensitizer into the conduction band of the semiconductor oxide, and η_{coll} is the electron collection efficiency. As ϕ_{inj} is proportional to k_{et}, to determine the effect of ultrafast injection dynamics on the final performance, it is necessary to estimate the contributions of LHE(λ) and η_{coll}. The contribution of the latter to the final IPCE is related to recombination processes, studied by means of photopotential measurements. LHE(λ) depends on the sensitizer band gap and loading, but in order to avoid its contribution to the IPCE, QDs of the same size have been used in all samples (DA and LA), and original IPCEs have also been normalized taking into account the amount of QDs involved. Figure 7A shows the IPCE prior to normalization, and Figure 7B shows the Kubelka−Munk transformation of reflectance measurements for these electrodes. A corrected IPCE is depicted in Figure S3 (Supporting Information). As expected, IPCE responses match quite well the absorption spectra of electrodes. Paying attention to Figure 7A, the best values have been obtained for DA-modified TiO_2 electrodes, showing similar values to those reported elsewhere.[21,28] Kongkanand et al.[16] obtained IPCE values around 20% (at excitonic peak wavelength) for CdSe sensitized TiO_2 electrodes using MPA as molecular wires, and Na_2S as electrolyte, which is in agreement with our results.

IPCE measurements have been performed in sulfite applying a fixed potential of 0.0 V to the photoanode during the experiment. Under these conditions, η_{coll} is maximized since the product of sulfite oxidation, sulfate, is not capable of efficiently withdrawing electrons from the photoanode, and the applied potential facilitates the extraction of electrons through

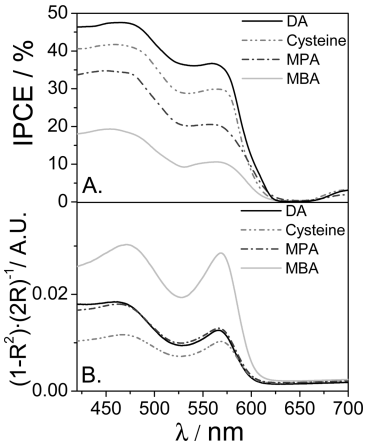

Figure 7. IPCE spectra for TiO_2 nanoporous electrodes sensitized with CdSe QDs using different modes of attachment in N_2-purged aqueous 0.5 M Na_2SO_3. Direct adsorption as well as linker-mediated adsorption (using cysteine, MPA, and MBA) are examined (A). Kubelka−Munk transformation corresponding to the diffuse reflectance spectra of the modified TiO_2 electrodes employed in the IPCE measurements (B).

TABLE 2: Photovoltaic Parameters of Closed Configuration Solar Cells

sample	j_{SC} (mA cm^{-2})[a]	V_{OC} (V)	FF[b]	efficiency (%)
DA, t_{ads} = 24 h	3.17	0.54	0.57	0.97
DA, t_{ads} = 48 h	4.59	0.56	0.58	1.49
DA, t_{ads} = 72 h	4.07	0.55	0.59	1.31
cysteine, t_{ads} = 72 h	2.73	0.51	0.44	0.61
MPA, t_{ads} = 72 h	3.16	0.53	0.52	0.86
MBA, t_{ads} = 72 h	2.47	0.49	0.47	0.56

[a] Short-circuit current. [b] Fill Factor.

the collector. This, in addition to the normalization of IPCE, leads to the corrected IPCE, which would be directly related to ϕ_{inj}.

As shown in Figure 7A, the best efficiencies have been obtained for DA and cysteine-mediated adsorption of colloidal QDs, but lower QD loading in the case of cysteine yields similar corrected efficiencies in both cases (Figure S3 in the Supporting Information). Otherwise, adsorption through MPA yields QD loadings similar to those for DA, but the resulting efficiency is much lower, leading to a low value in the normalized IPCE. Finally, when QDs are anchored with MBA, the highest amount of QDs is adsorbed, albeit minimum efficiency is obtained, revealing the lowest values in the corrected IPCE. As stressed above, the corrected IPCE can be easily connected to the previously discussed values of electron transfer rates. In fact, DA (for short adsorption times) and cysteine-assisted adsorption yield similar electron injection rate constant values ($k_{1,et}$ and $k_{2,et}$), higher than that corresponding to MPA. Finally, MBA presents the slowest injection. This is, as far as we know, the first illustration of a direct correlation between the corrected IPCE values and electron transfer kinetics on the picosecond-to-nanosecond time scale.

Solar Cell Measurements. Photovoltaic parameters in the closed cell configuration are summarized in Table 2. No particular post-treatment was done to the sensitized electrodes to facilitate the correlation of the different pieces of information. As observed, the direct adsorption method yields the best efficiency. It must be stressed that the adsorption time is a key parameter controlling photovoltaic performance. If adsorption is homogeneous (as in the case of linker mediated adsorption), long adsorption times are preferred to ensure the maximum fractional coverage of QDs on TiO_2. However, particularly in the case of DA, this is deleterious to the performance, because long adsorption times lead to QD aggregation and to the blockage of TiO_2 nanochannels.[21]

The overall performance of the solar cell mainly depends on the QD loading and the processes independently studied throughout this report, viz., electron transfer rate and recombination. Thereby, according to the results previously shown, DA yields the best performance in agreement with the favorable electron injection evidenced by the TG measurements, as well as minimum recombination revealed from photopotential relaxation experiments. On the other hand, tethering the same QDs (CdSe570) by means of linkers leads to a lower performance of the corresponding devices. Using cysteine as a molecular wire yields a low efficiency, probably because of the remarkable recombination between electrons and trapped holes, and lower amount of adsorbed QDs. Although electron injection through cysteine is faster than that via MPA, attaching QDs with the latter results in a better performance. This emphasizes the importance of the recombination with the electrolyte in the device. Finally, the lowest efficiency has been obtained when MBA is used as linker; this poor result can be ascribed both to a slow electron transfer, as it has been shown clearly by TG measurements, and to significant recombination as deduced from photopotential measurements.

Conclusions

In this work, we have proposed a new strategy to untangle the role of electron injection and electron−hole recombination processes in the performance of complete QDSCs. Importantly, techniques of different nature have been successfully combined to analyze separately the main processes (injection and recombination) that coexist in the operation conditions of the devices, giving a thorough interpretation of the cell efficiency. In summary, we have carried out sensitization of nanoparticulate TiO_2 electrodes by either direct and linker-assisted adsorption, testing, in addition, the effect of the QD size. A study of the subpicosecond-resolved dynamics of photogenerated carriers reveals that DA yields faster electron injection than LA. In the case of DA, remarkable TG signal dependence on adsorption time indicates different injection rates depending on the distance between the QDs and the oxide. Such a distribution of distances results from a random mechanism of adsorption and QD aggregation as described in previous papers.[21,22] With respect to the effect of QD size, regardless of the mode of attachment employed, the smaller the QD, the faster the electron injection. Interestingly, there is a direct correlation between electron injection rates and the IPCE values measured in the absence of electron acceptors in solution. Photopotential measurements unveil the slowest recombination rates when CdSe QDs are directly attached to TiO_2, both in the presence and in the absence of electron acceptors in solution. As expected, DA-sensitized electrodes yield in closed solar cell the best efficiencies. Lower cell efficiencies are obtained for LA samples, especially when MBA is used as a linker, on account of faster recombination and slower electron transfer.

Our study justifies that attaching QDs by the DA method improves the efficiency of devices as long as QD aggregation is avoided. Ongoing studies focus on the utilization of more open structures, such as TiO_2 nanotubes, allowing for a larger QD coverage for the DA method without aggregation as well as for a more efficient electron transport. Nonetheless, the mechanism of direct adsorption and the properties of QD/TiO_2 interfaces remain poorly understood.

In a more general vein, we have shown for the first time that there exists a direct correlation between the ultrafast carrier dynamics and the IPCE (corrected to take into account different QD loadings) in sulfite solutions, i.e., in the absence of electron acceptors in solution.

Acknowledgment. This work was partially supported by the Ministerio de Ciencia e Innovación of Spain, under the projects HOPE CSD2007-00007, MAT2009-14004 (Fondos FEDER), JES-NANOSOLAR PLE2009-0042, and MAT2007-62982, and by Generalitat Valenciana under the project PROMETEO/2009/058. Part of this research was supported by PRESTO program, Japan Science and Technology Agency (JST), Grant in Aid for Priority Area (470) (No.21020014), Scientific Research (No. 21310073) from the Ministry of Education, Sports, Science and Technology (MEXT) of the Japanese Government and Strategic Japan−Spain Cooperative Programs, JST. N.G. and S.G. also thank the Spanish Ministry of Education for the award of a FPU grant and a Ramón y Cajal contract, respectively.

Supporting Information Available: Kubelka−Munk transformation of reflectance spectra for LA-modified electrodes examined by the LF-HD-TG technique, electron lifetime measured in polysulfide, normalized IPCE, and fitting parameters for electrodes sensitized using CdSe512 and CdSe536. This material is available free of charge via the Internet at http://pubs.acs.org.

References and Notes

(1) Serpone, N.; Borgarello, E.; Grätzel, M. *J. Chem. Soc., Chem. Commun.* **1984**, *6*, 342–344.
(2) Gerischer, H.; Lübke, M. *J. Electroanal. Chem.* **1986**, *204*, 225–227.
(3) Vogel, R.; Pohl, K.; Weller, H. *Chem. Phys. Lett.* **1990**, *174*, 241–246.
(4) Liu, D.; Kamat, P. V. *J. Phys. Chem.* **1993**, *97*, 10769–10773.
(5) Vogel, R.; Hoyer, P.; Weller, H. *J. Phys. Chem. B* **1994**, *98*, 3183–3188.
(6) Zaban, A.; Micic, O. I.; Gregg, B. A.; Nozik, A. J. *Langmuir* **1998**, *14*, 3153–3156.
(7) Rühle, S.; Shalom, M.; Zaban, Z. *ChemPhysChem* **2010**, *11*, 2290–2304.
(8) Nozik, A. J. *Physica E* **2002**, *14*, 115–120.
(9) Nozik, A. J. *Chem. Phys. Lett.* **2008**, *457*, 3–11.
(10) Lee, Y.-L.; Lo, Y.-S. *Adv. Funct. Mater.* **2009**, *19*, 604–609.
(11) Fan, S.-Q.; Fang, J.; Kim, H.; Kim, J.-J.; Yu, J.-S.; Ko, J. *Appl. Phys. Lett.* **2010**, *96*, 063501.
(12) González-Pedro, V.; Xu, X.; Mora-Seró, I.; Bisquert, J. *ACS Nano* **2010**, *4*, 5783–5790.
(13) Cao, Y.; Bai, Y.; Yu, Q.; Cheng, Y.; Liu, S.; Shi, D.; Gao, F.; Wang, P. *J. Phys. Chem. C* **2009**, *113*, 6290–6297.
(14) Lee, H.; Leventis, H. C.; Moon, S.-J.; Chen, P.; Ito, S.; Haque, S. A.; Torres, T.; Nüesch, F.; Geiger, T.; Zakeeruddin, S. M.; Grätzel, M.; Nazeeruddin, Md. K. *Adv. Funct. Mater.* **2009**, *19*, 2735–2742.
(15) Barea, E. M.; Shalom, M.; Giménez, S.; Hod, I.; Mora-Seró, I.; Zaban, A.; Bisquert, J. *J. Am. Chem. Soc.* **2010**, *132*, 6834–6839.
(16) Kongkanand, A.; Tvrdy, K.; Takechi, K.; Kuno, M.; Kamat, P. V. *J. Am. Chem. Soc.* **2008**, *130*, 4007–4015.
(17) Robel, I.; Kuno, M.; Kamat, P. V. *J. Am. Chem. Soc.* **2007**, *129*, 4136–4137.
(18) Diguna, L. J.; Shen, Q.; Sato, A.; Katayama, A.; Sawada, T.; Toyoda, T. *Mater. Sci. Eng., C* **2007**, *27*, 1514–1520.
(19) Choi, J. J.; Lim, Y.-F.; Santiago-Berrios, M. B.; Oh, M.; Hyun, B.-R.; Sun, L.; Bartnik, A. C.; Goedhart, A.; Malliaras, G. G.; Abruña, H. D.; Wise, F. W.; Hanrath, T. *Nano Lett.* **2009**, *9*, 3749–3755.
(20) Yu, P.; Zhu, K.; Norman, A. G.; Ferrere, S.; Frank, A. J.; Nozik, A. J. *J. Phys. Chem. B* **2006**, *110*, 25451–25454.
(21) Guijarro, N.; Lana-Villarreal, T.; Mora-Seró, I.; Bisquert, J.; Gómez, R. *J. Phys. Chem. C* **2009**, *113*, 4208–4214.
(22) Giménez, S.; Mora-Seró, I.; Macor, L.; Guijarro, N.; Lana-Villarreal, T.; Gómez, R.; Diguna, L. J.; Shen, Q.; Toyoda, T.; Bisquert, J. *Nanotechnology* **2009**, *20*, 295204.
(23) Mora-Seró, I.; Giménez, S.; Fabregat-Santiago, F.; Gómez, R.; Shen, Q.; Toyoda, T.; Bisquert, J. *Acc. Chem. Res.* **2009**, *42*, 1848–1857.
(24) Robel, I.; Subramanian, V.; Kuno, M.; Kamat, P. V. *J. Am. Chem. Soc.* **2006**, *128*, 2385–2393.
(25) Mora-Seró, I.; Giménez, S.; Moehl, T.; Fabregat-Santiago, F.; Lana-Villarreal, T.; Gómez, R.; Bisquert, J. *Nanotechnology* **2008**, *19*, 424007.
(26) Lee, H.; Wang, M.; Chen, P.; Gamelin, D. R.; Zakeeruddin, S. M.; Grätzel, M.; Nazeeruddin, Md. K. *Nano Lett.* **2009**, *9*, 4224–4227.
(27) Fan, S.-Q.; Kim, D.; Kim, J.-J.; Jung, D. W.; Kang, S. O.; Ko, J. *Electrochem. Commun.* **2009**, *11*, 1337–1339.
(28) Guijarro, N.; Lana-Villarreal, T.; Shen, Q.; Toyoda, T.; Gómez, R. *J. Phys. Chem. C* **2010**, published online Nov 29, http://dx.doi.org/10.1021/jp105890x.
(29) Diguna, L. J.; Shen, Q.; Kobayashi, J.; Toyoda, T. *Appl. Phys. Lett.* **2007**, *91*, 023116.
(30) Hodes, G. *J. Phys. Chem. C* **2008**, *112*, 17778–17787.
(31) Burda, C.; Link, S.; Mohamed, M. B.; El-Sayed, M. *J. Chem. Phys.* **2002**, *116*, 3828–3833.
(32) Zhang, J. Z. *J. Phys. Chem. B* **2000**, *104*, 7239–7253.
(33) Klimov, V. I. *J. Phys. Chem. B* **2000**, *104*, 6112–6123.
(34) Klimov, V. I.; Schwarz, Ch. J.; McBranch, D. W.; Leatherdale, C. A.; Bawendi, M. G. *Phys. Rev. B* **1999**, *60*, R2177–R2180.
(35) Watson, D. F. *J. Phys. Chem Lett.* **2010**, *1*, 2299–2309.
(36) Gopidas, K.R.; Bohorquez, M.; Kamat, P. V. *J. Phys. Chem.* **1990**, *94*, 6435–6440.
(37) Blackburn, J. L.; Selmarten, D. C.; Nozik, A. J. *J. Phys. Chem. B* **2003**, *107*, 14154–14157.
(38) Blackburn, J. L.; Selmarten, D. C.; Ellingson, R. J.; Jones, M.; Micic, O.; Nozik, A. J. *J. Phys. Chem. B* **2005**, *109*, 2625–2631.
(39) Shen, Q.; Katayama, K.; Sawada, T.; Toyoda, T. *Thin Solid Films* **2008**, *516*, 5927–5930.
(40) Makhal, A.; Yan, H.; Lemmens, P.; Pal, S. K. *J. Phys. Chem. C* **2010**, *114*, 627–632.
(41) Sykora, M.; Petruska, M. A.; Alstrum-Acevedo, J.; Bezel, I.; Meyer, T. J.; Klimov, V. I. *J. Am. Chem. Soc.* **2006**, *128*, 9984–9985.
(42) Huang, J.; Stockwell, D.; Huang, Z.; Mohler, D. L.; Lian, T. *J. Am. Chem. Soc.* **2008**, *130*, 5632–5633.
(43) Matylitsky, V. V.; Dworak, L.; Breus, V. V.; Basché, T.; Wachtveitl, J. *J. Am. Chem. Soc.* **2009**, *131*, 2424–2425.
(44) Bang, J. H.; Kamat, P. V. *ACS Nano* **2009**, *3*, 1467–1476.
(45) Wang, Q.; Pan, D.; Jiang, S.; Ji, X.; An, L.; Jiang, B. *J. Cryst. Growth* **2006**, *286*, 83–90.
(46) Shen, Q.; Katayama, K.; Yamaguchi, M.; Sawada, T.; Toyoda, T. *Thin Solid Films* **2005**, *486*, 15–19.
(47) Yamaguchi, K.; Katayama, K.; Shen, Q.; Toyoda, T.; Sawada, T. *Chem. Phys. Lett.* **2006**, *427*, 192–196.
(48) Shen, Q.; Katayama, K.; Sawada, T.; Yamaguchi, M.; Toyoda, T. *Jpn. J. Appl. Phys.* **2006**, *45*, 5569–5574.
(49) Shen, Q.; Yanai, M.; Katayama, K.; Sawada, T.; Toyoda, T. *Chem. Phys. Lett.* **2007**, *442*, 89–96.
(50) Yu, W. W.; Qu, L.; Guo, W. Z.; Peng, X. G. *Chem. Mater.* **2003**, *15*, 2854–2860.
(51) Schaffner, M.; Bao, X.; Penzkofer, A. *Appl. Opt.* **1992**, *31*, 4546–4552.
(52) Dibbell, R. S.; Youker, D. G.; Watson, D. F. *J. Phys. Chem. C* **2009**, *113*, 18643–18651.
(53) Sambur, J. B.; Riha, S. C.; Choi, D.; Parkinson, N. A. *Langmuir* **2010**, *26*, 4836–4847.
(54) Zaban, A.; Greenshtein, M.; Bisquert, J. *Chem. Phys. Chem.* **2003**, *4*, 860–864.
(55) Monllor-Satoca, D.; Gómez, R. *J. Phys. Chem. C* **2008**, *112*, 139–147.
(56) Rajh, T.; Ostafin, A. E.; Micic, O. I.; Tiede, D. M.; Thurnauer, M. C. *J. Phys. Chem.* **1996**, *100*, 4538–4545.
(57) Grätzel, M. *Inorg. Chem.* **2005**, *44*, 6841–6851.

JP108499H